Journal of Neuroscience Methods 218 (2013) 148–160

Contents lists available at SciVerse ScienceDirect

Journal of Neuroscience Methods

journal homepage: www.elsevier.com/locate/jneumeth

Computational Neuroscience

Real-time automated spectral assessment of the BOLD response for neurofeedback at 3 and 7 T

Yury Koush[a,b,c,*], Mark A. Elliott[d], Frank Scharnowski[a,b], Klaus Mathiak[c,e,f]

[a] Department of Radiology and Medical Informatics, University of Geneva, Switzerland
[b] Institute of Bioengineering, École Polytechnique Fédérale de Lausanne (EPFL), Switzerland
[c] Department of Psychiatry, Psychotherapy and Psychosomatics, RWTH Aachen University, Germany
[d] Center for Magnetic Resonance and Optical Imaging (CMROI), Department of Radiology, University of Pennsylvania, USA
[e] JARA – Translational Brain Medicine, Germany
[f] Institute of Neuroscience and Medicine (INM-1), Research Center Jülich, Germany

HIGHLIGHTS

- Real-time single-voxel proton spectroscopy can assess T2* changes online.
- Real-time single-voxel proton spectroscopy is feasible at 3 T and at 7 T.
- FID optimized linear regression showed the highest sensitivity to BOLD.
- Water peak can be approximated with a single complex lorentzian line in real-time.

ARTICLE INFO

Article history:
Received 8 February 2013
Received in revised form 29 March 2013
Accepted 6 May 2013

Keywords:
Real-time
Feedback
Neurofeedback
fSVPS
MRS
fMRI
BOLD
High and ultra-high magnetic field
Time and frequency domain estimation

ABSTRACT

Echo-planar imaging is the dominant functional MRI data acquisition scheme for evaluating the BOLD signal. To date, it remains the only approach providing neurofeedback from spatially localized brain activity. Real-time functional single-voxel proton spectroscopy (fSVPS) may be an alternative for spatially specific BOLD neurofeedback at 7 T because it allows for a precise estimation of the local T2* signal, EPI-specific artifacts may be avoided, and the signal contrast may increase. In order to explore and optimize this alternative neurofeedback approach, we tested fully automated real-time fSVPS spectral estimation procedures to approximate T2* BOLD signal changes from the unsuppressed water peak, i.e. lorentzian non-linear complex spectral fit (LNLCSF) in frequency and frequency-time domain. The proposed approaches do not require additional spectroscopic localizers in contrast to conventional T2* approximation based on linear regression of the free induction decay (FID). For methods comparison, we evaluated quality measures for signals from the motor and the visual cortex as well as a real-time feedback condition at high (3 T) and at ultra-high (7 T) magnetic field strengths. Using these methods, we achieved reliable and fast water peak spectral parameter estimations. At 7 T, we observed an absolute increase of spectra line narrowing due to the BOLD effect, but quality measures did not improve due to artifactual line broadening. Overall, the automated fSVPS approach can be used to assess dynamic spectral changes in real-time, and to provide localized T2* neurofeedback at 3 and 7 T.

1. Introduction

Magnetic resonance spectroscopy (MRS) is one of the most commonly used approaches to explore brain neurochemistry (Ugurbil et al., 2003; Tkac et al., 2009; Alger, 2010; Nacewiz et al., 2012). In addition to quantifying changes in metabolite concentrations, MRS can also be used to investigate functional brain activity by means of the blood oxygen level dependent (BOLD) effect. To accomplish this, either line scan spectroscopic echo-planar imaging (EPI) can be used to obtain BOLD T2* brain maps (Weiskopf et al., 2003; Mulkern et al., 2004), or water proton ^{1}H MRS can be used to assess T2* from the unsuppressed water peak (Hennig et al., 1994; Richards et al., 1998; Zhu and Chen, 2001; Koush et al., 2011).

The BOLD signal from conventional functional magnetic resonance imaging (fMRI) based on gradient-echo (GE) EPI is dominated by large and small extravascular contributions. On the other hand, spin-echo (SE) fMRI at a TE close to the tissue T2 permits the suppression of the extravascular BOLD component from large

* Corresponding author at: Department of Radiology and Medical Informatics, University of Geneva, Rue Gabrielle-Perret-G. 4, CH-1211 Geneva, Switzerland. Tel.: +41 762015689.
E-mail address: yury.koush@unige.ch (Y. Koush).

0165-0270/$ – see front matter © 2013 Elsevier B.V. All rights reserved.
http://dx.doi.org/10.1016/j.jneumeth.2013.05.002

veins, allowing increased contributions from the microvasculature (Duong et al., 2003; Ugurbil et al., 2003; Hulvershorn et al., 2005). When using SE protocols in combination with ultra-high magnetic fields above 3 T, the extravascular effect from large draining veins can be diminished, and high spatial resolution microvasculature brain activation maps can be acquired (Duong et al., 2003; Ugurbil et al., 2003; Schafer et al., 2008; Budde et al., 2013). Functional water proton ^{1}H MRS based on a spin-echo acquisition has the same advantages as SE fMRI compared to the GE fMRI in terms of the microvasculature BOLD contributors at ultra-high magnetic field. However, SE fSVPS allows for a precise approximation of the T2* based on the acquired water protons spectra and FID (Zhu and Chen, 2001; Koush et al., 2011). In contrast, GE and SE protocols typically operate at a fixed TE approximated to the T2* and T2 of the tissue, respectively.

In addition to the acquisition sequence, the magnetic field strength can be used as well to study the BOLD mechanism in a more specific way. Spatial specificity and signal-to-noise ratio (SNR) are expected to improve at ultra-high magnetic field (Gati et al., 1997; Yacoub et al., 2003; van der Zwaag et al., 2009). The SNR, chemical shift dispersion, and quantification precision have been shown to increase when using ultra-high magnetic fields for MRS (Bartha et al., 2000; Ugurbil et al., 2003; Tkac and Gruetter, 2005; Tkac et al., 2009; Deelchand et al., 2010). This affords the ability to achieve the strong and stable water peak (Koush et al., 2011) along with the ability to consistently detect small concentration changes in metabolites (Mangia et al., 2006). However, ultra-high magnetic field results in stronger local field inhomogeneity and requires advanced adjustment and shimming procedures (Tkac and Gruetter, 2005).

Real-time applications require fast data acquisition and automated analysis. So far, this has been accomplished only for techniques such as electroencephalography (EEG), functional near-infrared spectroscopy (fNIRS), and EPI-based fMRI. These methods have certain advantages and disadvantages in comparison to each other (Ferrari et al., 2004; Cui et al., 2009). For example, on the one hand, EEG has a high temporal resolution, is less vulnerable to head movement artifacts, offers a silent measurement environment, is inexpensive, is widely available, and is portable. Real-time fMRI, on the other hand, has a high spatial resolution and can therefore provide region-specific neurofeedback (for reviews, see Weiskopf et al., 2004; Weiskopf, 2012; deCharms, 2008). Real-time fMRI-based neurofeedback has been used to train voluntary control over motor areas (Weiskopf et al., 2007; Bray et al., 2007; Subramanian et al., 2011), the anterior insular (Caria et al., 2007; Ruiz et al., 2013), emotion networks (Johnston et al., 2010), the right inferior frontal gyrus (Rota et al., 2009), the amygdala (Posse et al., 2003; Zotev et al., 2011), the anterior cingulate cortex (Weiskopf et al., 2003; deCharms et al., 2005; Mathiak et al., 2010), the visual cortex (Shibata et al., 2011; Scharnowski et al., 2012), and the auditory cortex (Yoo et al., 2006; Haller et al., 2010). To date, real-time fMRI remains the only method capable of providing neurofeedback from spatially localized activity across the entire brain in the millimeter range.

The potential of the individually specific SE fSVPS at high and ultra-high magnetic fields to explore the sensitivity to the precise T2* measures is of particular interest as a new type of the neurofeedback. Conventional single voxel proton MRS protocols typically require high or ultra-high magnetic field strengths, relatively large voxel sizes (~2–10 cm^3) as well as averaging over many repetition times (TRs) to achieve the sufficient spectra quality of the low-concentrated metabolites. This leads to comparatively long acquisition times, ranging from tens of seconds up to a few minutes (Bartha et al., 2000; Zhu and Chen, 2001; Mangia et al., 2006), which is suboptimal for real-time studies (Weiskopf et al., 2003). Functional water proton ^{1}H MRS acquisition differs from conventional MRS metabolite quantification, where the water peak is suppressed by either hardware or software manipulations (Haase et al., 1985; van der Veen et al., 2000), and can be adapted for real-time applications. To accomplish this, we selected the strongest water peak in the unsuppressed water spectra (Koush et al., 2011) and approximated T2* based on the free induction decay (FID) of the unsuppressed water peak by optimized linear regression (OLR). Our fSVPS acquisition protocol used a single voxel of 1 cm^3 and did not require averaging over multiple repetition times (TR = 1 s, TE = 22 ms, acquisition window = 256 ms). We measured BOLD signal changes in the primary motor cortex (PMC) and visual cortex (VC) at a high contrast-to-noise-ratio (CNR) and with sufficient statistical power (Koush et al., 2011). Furthermore, we demonstrated fSVPS feasibility to provide the real-time feedback signal from the PMC. Our approach, however, required an additional functional run to optimize the OLR approach.

For automatization of the real-time fSVPS, the choice of the single peak parameterization is particularly important, because high quantification precision as well as fast and stable estimation are required. Several time and frequency domain MR spectral quantification methods have been developed (for a review see Mierisova and Ala-Korpela, 2001; van den Boogaart et al., 1994). The automated multi-component linear combination model spectral fitting (LCModel), with the nearly model-free constrained regularization method reliably estimates difficult-to-distinguish metabolite peaks, and remains the most common approach for frequency domain spectral quantification (Provencher, 2001). The Levenberg–Marquardt non-linear least squares algorithm has been successfully used to fit complex spectra in the frequency domain, and it has been shown to perform better than linear methods (Mierisova and Ala-Korpela, 2001). It can be applied in the frequency domain for a set of fitting functions; for example, lorentzian, Gaussian or voigt (Marshall et al., 1997) line shapes. Mierisova and Ala-Korpela suggested that single lorentzian line non-linear fitting is sufficient for some applications, and can be applied if the water spectrum is dominant and if preprocessing is used to compensate for distortions in spectral line shapes. To compensate for these adverse effects, additional frequency and phase correction procedures can be applied (Klose, 1990; Tkac and Gruetter, 2005; Posse et al., 2007). Zhu and Chen (2001) suggested that the estimated water peak height, width, and the integral under the peak shape can be used as markers of different compartment contributions to the BOLD signal changes in spin-echo functional water proton MRS. However, increasing the number of components assigned to the single peak can yield physiologically implausible quantification and result in poor sensitivity of the dominant lorentzian line to the functional spectral changes (Singh et al., 1996).

We previously demonstrated the technical feasibility of the real-time fSVPS at 7 T which required a spectroscopic localizer to optimize the subsequent real-time run (OLR; Koush et al., 2011). The main focus of the present research was to develop a fully automated approach for neurofeedback studies based on the directly estimated, individual and localized T2* estimate using real-time fSVPS, and to optimize its sensitivity to T2* signal changes. To accomplish this, we investigated different water-peak estimation procedures and quantified T2* signal changes in terms of different spectral domain estimators, such as single peak width and height. These more recent T2* estimation approaches were compared to the more conventional OLR approach. Additionally, we performed an approximate evaluation of the T2 dynamics in order to explore the spin-echo differences using short TE protocols at high and ultra-high magnetic fields. The compared approaches were validated and evaluated at high (3 T) and ultra-high magnetic fields (7 T). Using quantitative quality measures such as *t*-statistics, contrast-to-noise ratio (CNR), and percent signal change (Δ%), we compared the quality of the feedback time courses and investigated if the

fSVPS estimation differs between brain regions (i.e. PMC and VC). A comparison with the well-established EPI is reasonable because most neurofeedback studies target a single ROI only, because EPI suffers from specific artifacts such as distortions or off-resonance effects, and because the direct estimation of T2* may lead to better specificity for the BOLD effect.

2. Methods

2.1. Data acquisition

fMRI and fSVPS data were acquired on a 3 T and a 7 T MR scanner (Siemens Medical Solutions, Erlangen, Germany). The scanners were equipped with a 12-channel phased array and single-channel quadrature head coil, respectively. Functional localizer data were acquired with a single-shot gradient-echo T2*-weighted EPI sequence with 300 repetitions (TR = 1000 ms, 16 slices volumes, matrix size 64 × 64, voxel size = 3 mm × 3 mm × 3.75 mm, flip angle $\alpha = 77^{\circ}$, bandwidth 2.23 kHz/pixel, TE = 30 ms at 3 T, TE = 28 ms at 7 T). For comparability, parameters were kept equal except TE that was slightly adapted to the shorter T2* at 7 T. Thresholded t-maps were obtained from a 30-s activation and 30-s baseline block design (details see below) for localization of the fSVPS voxels.

fSVPS data were acquired on the 3 T scanner using a spin-echo single voxel PRESS sequence with 300 repetitions (TE/TR = 30/1000 ms, flip angle $\alpha = 90^{\circ}/180^{\circ}/180^{\circ}$, bandwidth = 1 kHz, acquisition duration = 512 ms). Average voxel sizes were 9.9 mm × 11.6 mm × 10.5 mm for the motor condition and 10.7 mm × 11.6 mm × 10.5 mm for the visual condition. The 7 T spectroscopy protocol was slightly different, with TE/TR = 20/1000 ms, bandwidth = 2 kHz, acquisition duration = 256 ms, group average voxel sizes 9.0 mm × 10.3 mm × 10.5 mm for the motor condition, and 9.4 mm × 11.1 mm × 10.5 mm for the visual condition. The parameters were chosen to obtain a robust T2* estimate and the BOLD effect, but they were suboptimal for either of the acquisition methods, or field strengths. The fSVPS T2* estimates were hardly affected by the flip angle for the transversal magnetization, because the inversion pulses contribute to T1 saturation, the post-acquisition delay time is long compared to T2 of the tissue, and T2* estimates were calculated from the FID. For the fSVPS PRESS pulse sequence, TE was selected as short as feasible for 3 and 7 T in order to reduce T2 weighting and acquire early-echo data for precise T2* approximation. No water suppression was applied for the spectroscopy protocols. The first 10 acquisitions were discarded to avoid T1 saturation effects.

On both scanners, the real-time data export via local network was organized as described in Koush et al. (2011). The fSVPS data were exported online to a local PC and processed with custom-made real-time software (Koush et al., 2012). In order to improve the spectroscopic signal quality, we first performed a manual calibration of the transmitter amplitude. The optimization of the gradient shim currents was performed using first the automated Siemens "advanced" auto-shimming feature, followed by manual adjustment of the shim currents. On the 3 T scanner, the visual instructions and the feedback signal were shown to the participants via MR-compatible goggles (Resonance Technology Inc., Northridge, USA). On the 7 T scanner, they were projected onto an MR-compatible screen.

2.2. Participants

Two different groups of 7 healthy volunteers each were scanned on the 3 T scanner (4 male, 3 female, age 28 ± 7 years) and on the 7 T scanner (6 male, 1 female, age 33 ± 9 years), respectively. All participants were right-handed according to a minimal score of 6 on the Edinburgh Handedness Inventory (Oldfield, 1971). Study protocols were approved by the Ethics Committees of the Medical Faculty of the RWTH Aachen University and of the University of Pennsylvania. All participants gave written consent and were paid an allowance at the end of their participation.

2.3. Experimental design

The primary motor cortex (PMC) and the visual cortex (VC) are known to exhibit robust BOLD activation patterns and therefore were used to compare the sensitivity of the different data acquisition and estimation methods (Fig. 1). First, PMC and VC ROIs were functionally defined using functional localizer runs

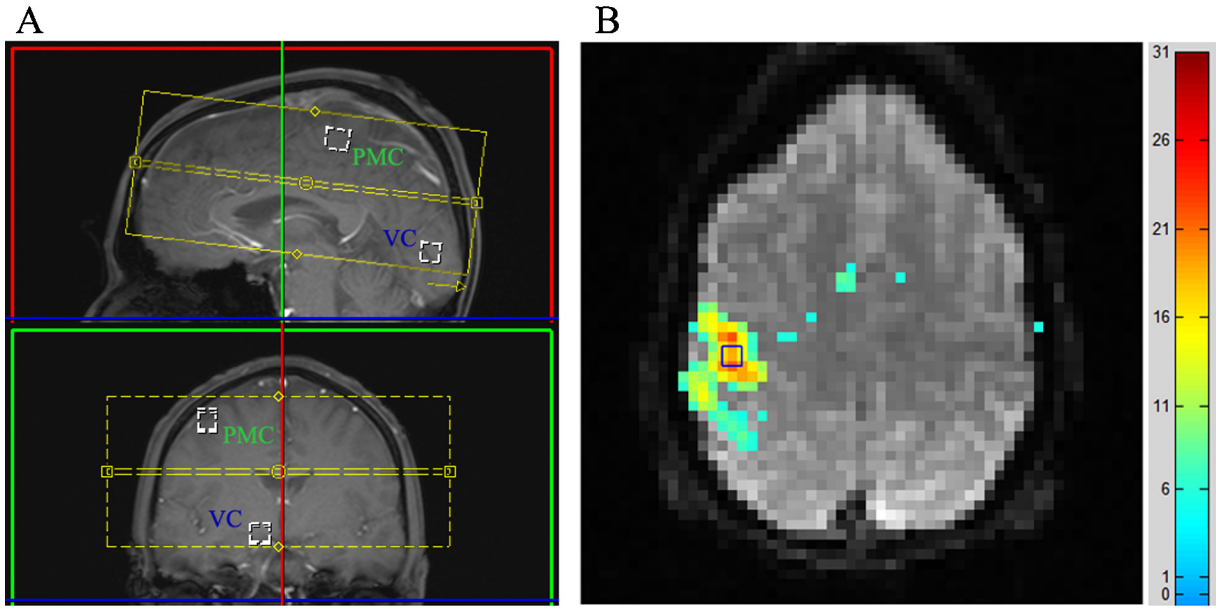

Fig. 1. Illustration of the selected ROIs. (A) PMC and VC ROIs are projected on sagittal (red) and coronal (green) planes for a typical participant. Dashed rectangles depict the EPI acquisition volume applied for the functional navigator (yellow). (B) Based on the BOLD activation maps from the functional PMC localizer, the spectroscopy voxel (blue) was selected across subsequent transverse EPI slices. EPI – echo-planar imaging, ROI – region of interest, PMC – primary motor cortex, VC – visual cortex. (For interpretation of the references to color in this figure legend, the reader is referred to the web version of the article.)

with subsequent statistical brain mapping (t-statistics). To localize the right PMC ROI, the participants performed 5 blocks of finger tapping with their left hand interleaved with 5 baseline blocks. During baseline blocks the participants were asked to look at the fixation point. Each block lasted 30 s, resulting in 5 min total run duration. The VC functional localizer paradigm had the same timeline as the PMC localizer, but instead of finger tapping, we presented a flickering square checkerboard (100% contrast, 6 Hz contrast reversal) covering the whole screen ($\sim 25^\circ \times 30^\circ$ visual angle). Based on these functional localizers, we then defined the fSVPS single-voxel so that it covered the most active part of the respective ROI (size approximately 1 cm × 1 cm × 1 cm; see Fig. 1B).

Once the fSVPS voxel was defined, participants performed runs that were identical to the functional localizer runs, but this time using the fSVPS acquisition method. Finally, we provided real-time feedback from the PMC using fSVPS. For this, participants were instructed to adjust their finger tapping so that a green horizontal bar (which represented their PMC ROI activity) would move up to the level of a predefined red horizontal target bar. During baseline blocks, the red bar was close to the fixation point; during regulation blocks, the red bar was presented at the upper part of the screen which corresponded to 100% of the dynamic normalization range (for details see Koush et al., 2012). During feedback blocks, participants attempted to maximize the feedback of the PMC activity by tapping their fingers at different speeds or strengths.

2.4. Real-time feedback signal extraction and processing

The real-time fSVPS feedback signal was estimated in the time domain as apparent T2* changes from the unsuppressed water peak. The water peak was first zero-frequency shifted, Gaussian filtered, and phase-corrected (Klose, 1990; Tkac and Gruetter, 2005). To allow for real-time fSVPS feedback, optimized linear regression (OLR) of the logarithm of the free induction decay $\ln(|FID|)$ from the single voxel was applied (Koush et al., 2011). The optimal linear regression length was estimated from the previously acquired spectroscopic PMC functional run without feedback and then used for the subsequent real-time run. Further details about the feedback signal processing can be found in Koush et al. (2011). Note, that the first fSVPS acquisition is not required for feedback signal based on the proposed automated LNLCSF approach. However, for comparison purposes we used the same experimental pipeline and feedback signal estimation as for the OLR approach.

The feedback signal was extracted from spectroscopic data after each FID acquisition. After the signal was extracted, we used a custom-made toolbox to remove the feedback signal drifts, to detect and correct spikes, to remove high frequency noise, and to normalize the signal (Koush et al., 2012; the toolbox was extended for spectroscopic information and is available on request from the corresponding author). All computations were carried out on a standard PC with Matlab 7.10 (The Mathworks, Natick, MA).

For the spectroscopy acquisitions, we did not take the participants' head motion-induced variation into account. However, to ensure that motion artifacts did not cause significant signal distortions, we located relatively small ROIs within large active zones of the PMC or VC. We controlled the participant head displacements between the fSVPS experimental runs with intermediate EPI scans which were acquired before and after the fSVPS runs and realigned to the ROI template volume (<1 mm, SPM8).

2.5. Applied T2* estimation approaches

We compared three different T2* approximation approaches in terms of their sensitivity to BOLD signal changes of the PMC and VC time courses: (1) statistically optimized linear regression (OLR; Koush et al., 2011); (2) automated single (dominant) lorentzian non-linear complex spectral fit (LNLCSF; van den Boogaart et al., 1994); and (3) back-transformed parameterization of the single lorentzian line estimated in (2). All of these methods were evaluated in terms of the estimated absolute T2* measures induced by the water peak dynamics, time series t-value, CNR, and the percent signal changes (Δ%) of the experimental runs. The comparison analysis was performed separately for the 3 T and the 7 T scanner.

Statistically optimized linear regression was applied to the acquired free induction decay function (FID) in the time domain. In the time domain, FID can be represented as a sum of exponentially damped sinusoids. By assuming that the joint water is the dominating component in the acquired spectra, the natural logarithm of the FID can be simplified:

$$\ln(\mathrm{FID}) = -\frac{t}{\mathrm{T2}^*_{\mathrm{water}}} + \ln(A_{\mathrm{water}}) + i\phi_{\mathrm{water}} \quad (1)$$

with the T2* of the joint water signal changes, amplitude A, and phase ϕ. OLR for individual regression lengths was applied to approximate the experimental logarithmic curve for providing a T2* estimate. Despite its simplicity, the proposed estimation approach can provide reliable and robust estimates of the T2* changes at ultra-high magnetic fields (Koush et al., 2011).

Automated single (dominant) lorentzian non-linear complex spectral fit was applied to the Fourier-transformed FID in the frequency domain. In the frequency domain, the mono-exponential unsuppressed water peak is a lorentzian line $F(\nu_w)$ whose real part is:

$$Re\{F(\nu_w)\} = \frac{h^2 I}{h^2 + 4(\nu_w - \nu)^2}\cos(\phi) + \frac{2hI(\nu_w - \nu)}{h^2 + 4(\nu_w - \nu)^2}\sin(\phi) \quad (2)$$

with half lorentzian line width h, intensity I, phase angle ϕ and resonance frequency ν. The imaginary part of the estimation function $F(\nu_w)$ is similar to Eq. (2) with the sine and cosine terms reversed (van den Boogaart et al., 1994). An automated single lorentzian non-linear complex fit was performed using the Levenberg–Marquardt non-linear fitting algorithm applied separately to the real and to the imaginary parts of the complex spectra (van den Boogaart et al., 1994). As raw spectra were filtered using a Gaussian filter, the estimation function was additionally weighted with the corresponding filter coefficients. We derived T2* from the approximated real part of the complex lorentzian line in the frequency domain ($\mathrm{T2}^* = 1/(\pi \cdot 2 \cdot h)$).

Subsequently, we applied the back-transformed parameterization of the single lorentzian line estimated with LNLCSF approach in the frequency domain. To accomplish this, fitted real and imaginary data were combined and back-transformed into the time domain. The resultant single-exponential signal was linearized by taking the logarithm natural $\ln(|FID|)$ in order to approximate the T2* value in the same way as for the OLR approach and to keep the same T2* dimension. This constituted the T2* estimation by the LNLCSF in combination with a subsequent time domain linear regression.

In order to evaluate alternatives to the OLR and LNLCSF spectral width estimates, we also included the water peak height as a quantification parameter. We also explored the multiple lorentzian parameterizations to address the possible underfitting of additional water peaks (Singh et al., 1996). The automated water peak parameterization was configured once for 3 T and for 7 T data.

2.6. Time courses' quality measures

As quality measures, t-statistics, CNR, and percent signal change (Δ%) were calculated for all the acquired time courses. This allowed for comparison of the acquisition methods and the feedback signal estimation approaches at 3 and at 7 T. For the statistical analysis of the BOLD signal changes in the respective functional data, we specified general linear models (GLM) with regressors for the

experimental conditions, i.e. boxcar time series representing baseline and finger tapping/visual stimulation blocks convolved with the canonical hemodynamic response function in SPM8 (Welcome Trust Centre for Neuroimaging, UK). Each participant's motion parameters were included into the GLM as nuisance regressors. Motion parameters for the spectroscopy acquisitions were not available. To calculate the CNR we estimated the differences between the signal means during baseline and activation conditions, as well as the residual variances. Percent signal changes were calculated in an event-wise manner.

3. Results

As described above, we acquired fSVPS data at 3 T and at 7 T from the PMC, from the VC, and from the PMC with feedback (PMC NF) runs. The real-time calculation of the feedback signal during the PMC NF runs was based on the OLR approach. For the offline analysis, the data from all three conditions (PMC, VC, PMC NF) were analyzed with the OLR as well as with an automated estimation of T2* from the water peak using frequency and time (back-transformed) domain LNLCSF.

3.1. Spectral quality and explicit T2* estimation based on the OLR approach at 3 and at 7 T

In this section, we evaluated the spectra preprocessing steps, and the feasibility of the OLR T2* estimation at 3 and at 7 T. The water signal contains contributions from different tissue compartments within the single acquisition voxel that differ slightly in their spectral representation. At 3 T, the water peaks appear free of distortions and have an almost symmetric shape (Fig. 2A), which can be well-fitted by a single lorentzian line. At 7 T, the water peaks are often distorted due to eddy currents, poor shimming due to large local field inhomogeneities, etc. (Fig. 2B). Accordingly, the effects of preprocessing were more noticeable in the 7 T acquisitions (Fig. 2B). The group average of the OLR estimated time courses is shown in Fig. 3. It shows that performance was highly consistent across participants and ROIs.

The individual averages of the acquired time courses represent the variability in T2* values between participants as well as between ROI time courses at 3 and at 7 T (Table 1). The mean T2* values reflected relatively high but still realistic values at 3 and rather low values at 7 T. The between subject variance of T2* appeared larger for the participants that were scanned on the 7 T scanner compared to those on the 3 T scanner.

Percent signal changes during activation compared to baseline revealed a high sensitivity of the fSVPS acquisition to the BOLD signal changes at 3 T ($\Delta\%T2^*_{PMC} = 4.1 \pm 1.6$, $\Delta\%T2^*_{PMC\ NF} = 5.7 \pm 2.5$, $\Delta\%T2^*_{VC} = 5.4 \pm 1.4$) as well as at 7 T ($\Delta\%T2^*_{PMC} = 4.5 \pm 2.3$, $\Delta\%T2^*_{PMC\ NF} = 5.3 \pm 2.0$, $\Delta\%T2^*_{VC} = 3.5 \pm 2.2$). There is no significant difference of the OLR estimated percent signal change between the 3 T and the 7 T data (paired one-tailed t-test, $df = 20$; $t = 1.0$, $p > 0.2$). However CNR values reveal a significantly higher BOLD sensitivity of the 3 T as compared to the 7 T fSVPS (paired one-tailed t-test, $df = 20$; $t = 4.0$, $p < 0.001$; Table 2).

The group average of the water peak line width was approximately 3-times higher at 7 T (PMC: 23.7 ± 10.2 Hz, PMC NF: 22.3 ± 12.5 Hz, VC: 19.8 ± 5.5 Hz) compared to 3 T (PMC: 6.0 ± 0.5 Hz, PMC NF: 5.9 ± 0.6 Hz, VC: 7.8 ± 1.3 Hz). The much broader water peak at 7 T suggests that shimming conditions or

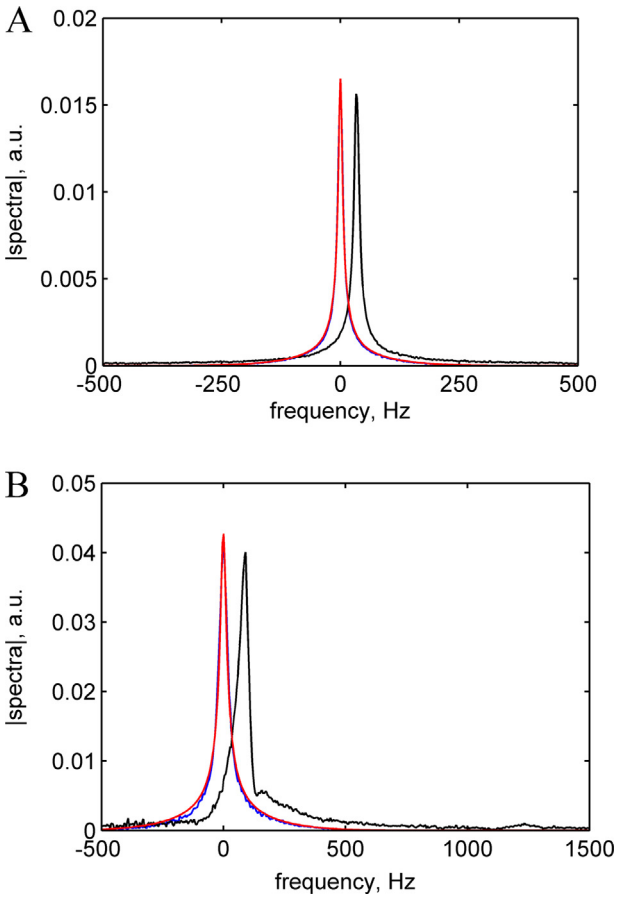

Fig. 2. Examples of parameterized VC magnitude spectra at 3 T (A) and at 7 T (B). Original spectra (black) were first preprocessed (blue) using Gaussian filter, center-frequency shift, eddy current compensation, and phase-correction. Subsequently, the spectra were fitted (red) with the automated LNLCSF approach. Fat peak and water peak distortions, particularly in the 7 T spectrum, were successfully eliminated. VC – visual cortex, LNLCSF – lorentzian non-linear complex spectral fit. (For interpretation of the references to color in this figure legend, the reader is referred to the web version of the article.)

Table 1
Direct T2* measures in *ms* at 3 and at 7 T magnetic fields.

Subject[a]	3 T			7 T		
	PMC	PMC NF	VC	PMC	PMC NF	VC
1	53.0 ± 0.7	51.3 ± 0.9	46.5 ± 1.5	8.3 ± 0.3	7.2 ± 0.4	12.0 ± 0.1
2	44.4 ± 1.4	46.1 ± 2.1	43.1 ± 1.5	10.4 ± 0.4	21.7 ± 0.9	19.2 ± 0.3
3	53.1 ± 1.2	57.2 ± 2.1	32.7 ± 0.9	18.4 ± 0.3	17.2 ± 0.2	30.7 ± 0.6
4	53.5 ± 0.8	51.2 ± 1.1	34.2 ± 1.2	21.3 ± 0.7	27.5 ± 0.6	14.1 ± 0.2
5	53.8 ± 1.4	62.7 ± 1.6	49.3 ± 1.1	9.9 ± 0.6	8.8 ± 0.5	16.9 ± 0.8
6	55.2 ± 1.0	51.6 ± 1.5	46.2 ± 0.8	29.2 ± 0.9	22.3 ± 0.5	17.2 ± 0.6
7	58.2 ± 0.8	58.6 ± 0.9	38.6 ± 1.2	14.9 ± 0.2	16.4 ± 0.4	12.7 ± 0.3
Group average	53.0 ± 4.2	54.1 ± 5.7	41.5 ± 6.5	16.1 ± 7.5	17.3 ± 7.3	17.5 ± 6.4

[a] The group of participants was different at 3 T and at 7 T. The SD was estimated separately for each time course and then averaged across the participants. PMC – primary motor cortex; PMC NF – primary motor cortex with feedback; VC – visual cortex.

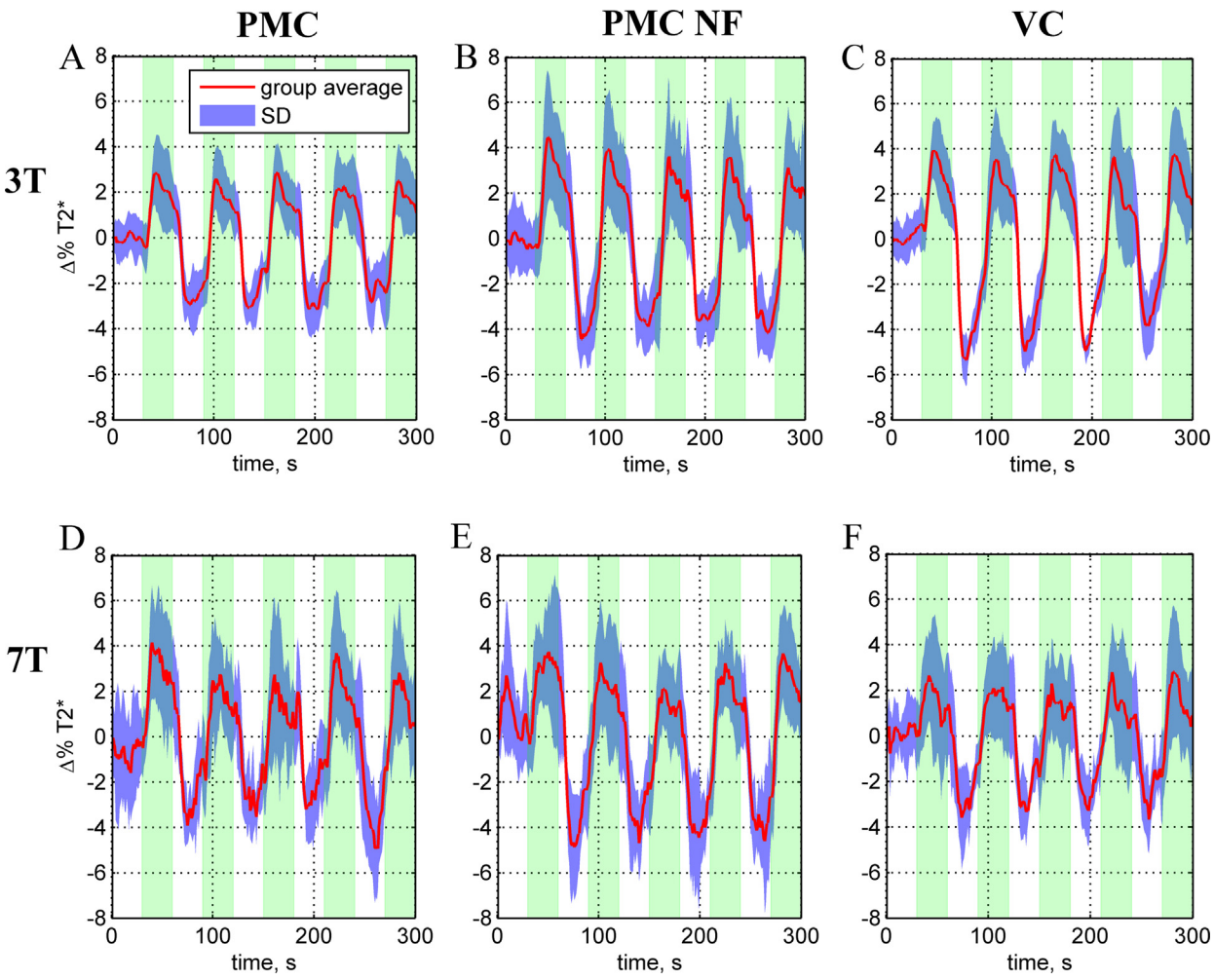

Fig. 3. Relative change of T2* in the fSVPS time courses at 3 and at 7 T based on OLR. Red lines show the average T2* signal change across participants for the PMC (A, D), the PMC NF (B, E), and the VC (C, F) condition at 3 T (A, B, C) and at 7 T (D, E, F). The shaded blue area marks standard deviation (SD) across the group. The 7 T data generally show comparable Δ%T2* but larger SD. PMC – primary motor cortex, PMC NF – primary motor cortex with feedback, VC – visual cortex, SD – standard deviation. (For interpretation of the references to color in this figure legend, the reader is referred to the web version of the article.)

signal stability were not optimal despite the shimming procedures applied at the ultra-high field scanner.

3.2. Comparison of the T2* estimations

In this section, we evaluated an optimal water peak T2* estimate for real-time fSVPS studies which does not require additional fSVPS optimization runs, but which can be configured once for a given magnetic field strength. To accomplish this, we compared our quantitative quality measures for the OLR approach, the automated frequency domain LNLCSF approach, and the automated time domain LNLCSF approach. In artifact-free data, the OLR and LNLCSF approaches should not result in significant T2* estimation differences. However, we observed such differences because of nonlinearities that were present in the estimated signal (Fig. 4).

Significantly higher t-values were obtained at 3 T as compared to 7 T (paired one-tailed t-test; PMC: $t = 2.7$, $p < 0.02$, df = 6; PMC NF: $t = 6.1$, $p < 0.001$, df = 6; VC: $t = 2.7$, $p < 0.02$, df = 6; see also Table 3, first level activation threshold, $p < 0.001$).

Table 2
CNRs of the OLR-estimated time courses for each participant.

Session/Subject[a]	3 T			7 T		
	PMC	PMC NF	VC	PMC	PMC NF	VC
1	2.7	2.7	3.4	1.5	1.7	0.9
2	2.6	3.3	4.9	0.6	2.7	1.6
3	3.6	5.3	2.8	2.2	2.6	0.9
4	3.3	4.7	1.4	5.4	4.9	2.0
5	3.3	3.2	2.5	2.8	1.1	2.8
6	2.4	2.5	3.3	1.0	1.8	3.4
7	4.1	3.6	4.4	1.9	2.2	1.9
Group average	3.1 ± 0.6	3.6 ± 1.0	3.2 ± 1.2	2.2 ± 1.6	2.4 ± 1.2	1.9 ± 0.9

[a] The group of participants was different at 3 T and at 7 T. PMC – primary motor cortex; PMC NF – primary motor cortex with feedback; VC – visual cortex.

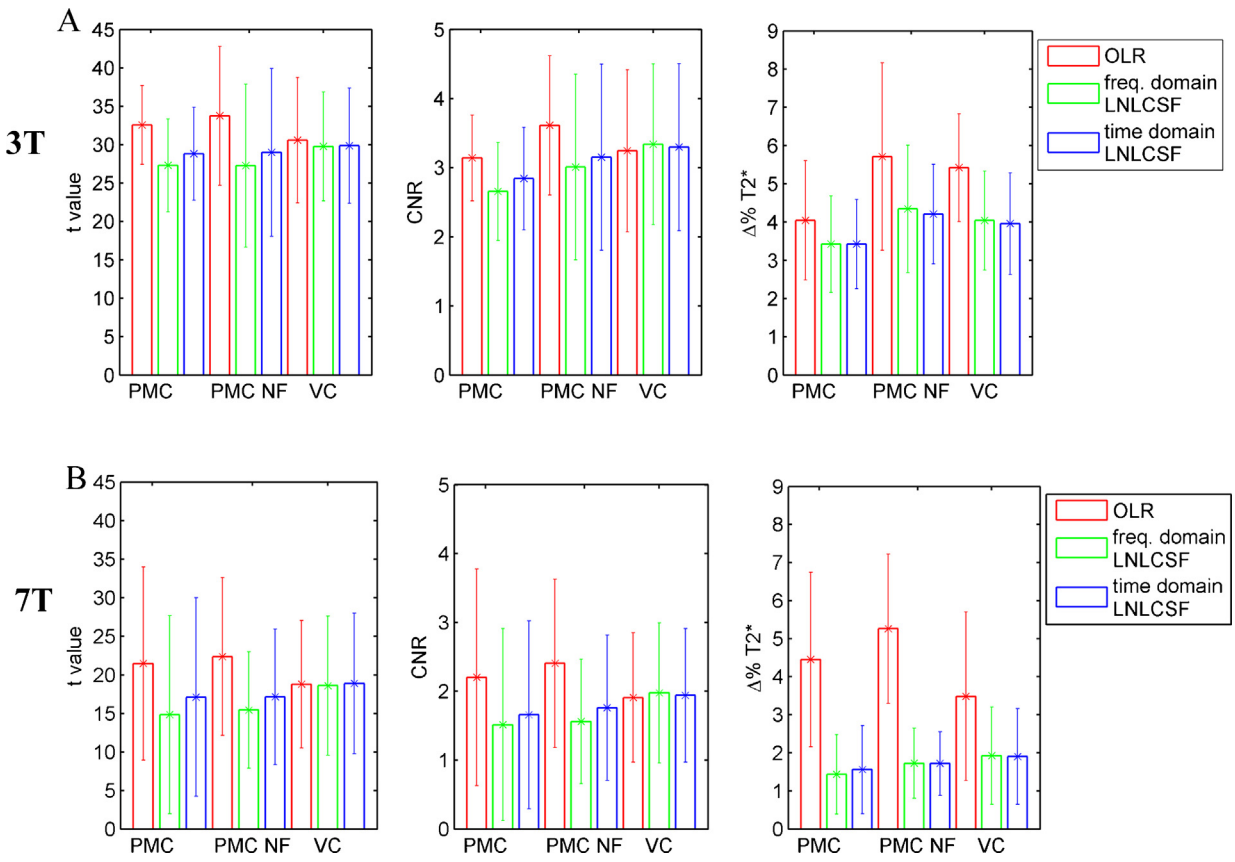

Fig. 4. Comparison of quality measures for the estimated T2* time courses. T2* estimations based on the OLR (red bars), the automated frequency domain LNLCSF (green bars), and the automated time domain LNLCSF (blue bars) were compared across the different ROIs for 3 T (A) and 7 T (B). In most cases, the OLR approach resulted in higher *t*-statistics, CNR, and percent signal changes than the LNLCSF approaches. This was pronounced for the percent T2* change (Δ%T2*) at 7 T (B). Error bars represent the standard deviation. OLR – optimized linear regression, LNLCSF – lorentzian non-linear complex spectral fit, PMC – primary motor cortex, PMC NF – primary motor cortex with feedback, VC – visual cortex. (For interpretation of the references to color in this figure legend, the reader is referred to the web version of the article.)

Moreover, the OLR approach resulted in significantly higher *t*-values than the time domain LNLCSF approach for the PMC and the PMC NF conditions (paired one-tailed *t*-test; PMC 3 T: $t = 4.3$, $p < 0.005$, $df = 6$; PMC 7 T: $t = 2.3$, $p < 0.05$, $df = 6$; PMC NF 3 T: $t = 3.7$, $p < 0.005$, $df = 6$; PMC NF 7 T: $t = 3.0$, $p < 0.01$, $df = 6$). Further, the time domain LNLCSF approach resulted in significantly higher *t*-values than the frequency domain LNLCSF approach (paired one-tailed *t*-test; PMC 3 T: $t = 2.5$, $p < 0.05$, df = 6; PMC 7 T: $t = 3.2$, $p < 0.01$, df = 6; PMC NF 3 T: $t = 4.6$, $p < 0.005$, df = 6; PMC NF 7 T: $t = 2.2$, $p < 0.05$, df = 6). The frequency domain estimation of the T2* was computed from just the real part of the complex spectra leading to the inferiority of this method. Interestingly, there were no significant differences between the three approaches for the VC time courses, which indicates that the imaginary part of the complex spectral width had less of an effect on the T2* estimate in the occipital ROI (paired one-tailed *t*-test; 3 T: $t = 0.2$, $p = 0.43$, df = 6; 7 T: $t = 0.8$, $p = 0.24$, df = 6).

CNRs provide an additional quality measure of the estimation approaches. The pattern of results for the CNRs was the same as obtained for the *t*-values (Fig. 4 second column; Table 4). For the PMC and for the PMC NF time courses, the OLR approach resulted in a higher CNR than the LNLCSF approaches (paired one-tailed *t*-test; PMC 3 T: $t = 2.6$, $p < 0.05$, $df = 6$, $df = 6$; PMC 7 T: $t = 3.0$, $p < 0.01$, $df = 6$; PMC NF 3 T: $t = 2.2$, $p < 0.05$, $df = 6$; PMC NF 7 T: $t = 1.7$, $p < 0.10$, $df = 6$). For the VC time courses, no significant differences were observed (paired one-tailed *t*-test; 3 T: $t = 0.3$, $p = 0.40$; 7 T: $t = 0.3$, $p = 0.39$). Also, the CNR of the time domain LNLCSF T2* estimates was significantly higher than those of the frequency LNLCSF (paired one-tailed *t*-test, df = 6) for the PMC (3 T: $t = 2.8$, $p < 0.05$, $df = 6$; 7 T: $t = 2.2$, $p < 0.05$, $df = 6$), for the PMC NF (3 T: $t = 2.5$, $p < 0.05$; 7 T: $t = 1.9$, $p < 0.05$), but was not significant for the VC time courses (3 T: $t = 0.6$, $p = 0.28$; 7 T: $t = 0.7$, $p = 0.25$).

Percent signal change is an estimate for effect size and showed the same pattern of results as the statistical markers (Fig. 4 third column; Table 5). The OLR approach resulted in higher percent signal changes than both LNLCSF approaches for all conditions (paired one-tailed *t*-test, df = 6) at 3 T (PMC: $t = 2.1$, $p < 0.05$; PMC NF: $t = 2.7$, $p < 0.05$; VC: $t = 4.9$, $p < 0.02$) and at 7 T (PMC: $t = 4.0$, $p < 0.005$; PMC

Table 3
t-values of the OLR, the frequency LNLCSF, and the time domain LNLCSF estimated T2* time courses (first level activation statistics, $p < 0.001$).

Group average[a]	3 T			7 T		
	PMC	PMC NF	VC	PMC	PMC NF	VC
OLR	32.6 ± 5.1	33.8 ± 9.0	30.6 ± 8.2	21.4 ± 12.5	22.4 ± 10.2	18.8 ± 8.2
Freq. domain LNLCSF	27.3 ± 6.1	27.3 ± 10.6	29.9 ± 7.1	14.8 ± 12.8	15.4 ± 7.5	18.6 ± 9.0
Time domain LNLCSF	28.8 ± 6.1	29.0 ± 10.9	29.8 ± 7.5	17.1 ± 12.9	17.1 ± 8.8	18.9 ± 9.1

[a] The group of participants was different at 3 T and at 7 T. PMC – primary motor cortex; PMC NF – primary motor cortex with feedback; VC – visual cortex.

Table 4
CNRs of the OLR, the frequency LNLCSF, and the time domain LNLCSF estimated T2* time courses.

Group average[a]	3 T			7 T		
	PMC	PMC NF	VC	PMC	PMC NF	VC
OLR	3.1 ± 0.6	3.6 ± 1.0	3.2 ± 1.2	2.2 ± 1.6	2.4 ± 1.2	1.9 ± 0.9
Freq. domain LNLCSF	2.7 ± 0.7	3.0 ± 1.3	3.3 ± 1.2	1.5 ± 1.4	1.6 ± 0.9	2.0 ± 1.0
Time domain LNLCSF	2.8 ± 0.7	3.2 ± 1.4	3.3 ± 1.2	1.7 ± 1.4	1.8 ± 1.1	1.9 ± 1.0

[a] The group of participants was different at 3 T and at 7 T. PMC – primary motor cortex; PMC NF – primary motor cortex with feedback; VC – visual cortex.

NF: $t = 5.0$, $p < 0.005$; VC: $t = 4.1$, $p < 0.005$). Time and frequency domain LNLCSF approaches obtained comparable percent signal changes.

Based on the OLR approach, the average narrowing of the line width during activation was more than 3-times higher in the PMC, and about 1.6 times higher in the VC at 7 T (PMC: 1.07 ± 0.80 Hz, PMC NF: 1.25 ± 0.95 Hz, VC: 0.69 ± 0.44 Hz) compared to 3 T (PMC: 0.25 ± 0.12 Hz, PMC NF: 0.34 ± 0.17 Hz, VC: 0.43 ± 0.13 Hz).

To compare the reliability of OLR, frequency LNLSCF, and time LNLCSF estimation, event related responses were estimated. The individual time courses were normalized and averaged separately for each condition (PMC, PMC NF, and VC) and for the 3 and the 7 T data. The event-related averages showed hardly any difference, neither between the three estimation approaches, the 3 runs, nor between the scanners (Fig. 5). The only difference we found was an increased variance on the 7 T scanner. The estimation procedures therefore seemed to be unbiased but showed differences in stability.

Generally, the water peak height does not provide an estimation of the absolute T2* values. Indeed, we found that the estimated height of the water peak showed lower CNRs than the water peak width CNRs at 3 T ($CNR_{PMC} = 2.6 \pm 0.6$, $CNR_{PMC\ NF} = 2.8 \pm 1.4$, $CNR_{VC} = 3.5 \pm 1.4$) and at 7 T ($CNR_{PMC} = 1.3 \pm 1.1$, $CNR_{PMC\ NF} = 1.3 \pm 0.9$, $CNR_{VC} = 2.2 \pm 1.0$).

The applied single-lorentzian LNLCSF estimation of the 7 T data might have resulted in larger absolute T2* and lower Δ%T2* values due to underfitting of additional peaks. In order to address this bias, we explored the multiple lorentzian parameterization. However, due to the variable shapes of the measured water peaks, this analysis revealed inconsistent parameter estimates for most of the time courses. The procedure often resulted in a mathematically optimal but physiologically implausible parameterization. A solution for this problematic parameterization might be to improve the spectroscopy acquisition quality rather than compensating nonlinearity with multiple parameter fits.

3.3. T2* and T2 BOLD dynamics evaluation

Two parameters characterize a mono-exponential decay of the *FID*. First, the decay rate of the *FID* is represented by T2*: $|FID| = I_0 \cdot \exp(-t/T2^*)$; note that in our fSVPS pulse sequence, the SE data acquisition starts at TE (Fig. 6; $t = 0$). Second, the initial amplitude I_0 follows a T2/T1-contrast. The event related group averages of the preprocessed $|FID|$ for the 3 T and the 7 T data are shown in Fig. 6A–C. We calculated the normalized $|FID|$ differences (Fig. 6D–F; $\Delta|FID| = |FID|_{activation} - |FID|_{baseline}$), which reflected slower *FID* decay rate in the activation condition at 3 T and additional I_0 effects at 7 T. In order to assess the local sensitivity maxima more precisely, the differential curves were zero-phase filtered (Butterworth low-pass filter, $Fc_{3T} = 0.03$ Hz, $Fc_{7T} = 0.02$ Hz; order = 5; bold curves in Fig. 6 D-F).

We estimated respective T2* sensitivity maxima of the $\Delta|FID|$ curves for the PMC (3 T: 1.7% at 30 ms; 7 T: 1.3% at 12 ms), for the PMC NF (3 T: 2.2% at 30 ms; 7 T: 1.9% at 16 ms), and for the VC (3 T: 3.1% at 19 ms; 7 T: 2.3% at 10 ms) time courses (Fig. 6 D-F).

Given I_0 measures, percent T2 changes (ΔT2) can be approximated neglecting the T1 effect using $T2 \sim -TE/\ln(I_0)$. Note that our T2 estimation is applied for a shorter than canonical spin-echo TE used for T2 contrast and can be biased if the *FID* contains multiple exponential components particularly in 7 T data. Group averaged ΔT2 was evaluated for the PMC (3 T: 0.10 ± 0.05%; 7 T: 0.09 ± 0.10%), the PMC NF (3 T: 0.11 ± 0.07%; 7 T: 0.08 ± 0.14%), and the VC condition (3 T: 0.24 ± 0.09%; 7 T: 0.22 ± 0.18%). The ΔT2 estimates were much smaller that ΔT2* and did not differ between 3 T and 7 T (paired, one-tailed *t*-test, $t = 0.68$, $p = 0.46$).

3.4. Computation time for real-time fSVPS

Average processing time was 4.6 ms for each spectrum using the standard preprocessing operations as they were described in Section 2 (Matlab 7.10, CPU Intel Core i7-2620M 2.7 GHz, 4 GB RAM). Preprocessed spectra and stable convergence of the Levenberg–Marquardt non-linear fitting algorithm made LNLCSF feasible for automated and fast estimation of the single water peak parameters. For the T2* estimation, the computational speed varied slightly between the three different approaches: OLR 1 ms, frequency domain LNLCSF 9.5 ms, and time domain LNLCSF 10.3 ms. There is an additional delay of <30 ms until the spectra file is released from the scanner so that the spectra FID series from the Siemens MRIR can be exported. Thereby feedback was given latest 50 ms after acquisition of the spectrum (TR = 1 s).

4. Discussion

Single-voxel proton spectroscopy and applied T2* estimation approaches can measure functional T2* changes in real-time at 3 and 7 T. Despite the unsatisfactory line-width at 7 T, OLR proved to be the most robust approach in the both settings. However, LNLCSF is more suited for real-time applications such as localized neurofeedback.

Table 5
Δ% of the OLR, the frequency LNLCSF, and the time domain LNLCSF estimated T2* time courses.

Group average[a]	3 T			7 T		
	PMC	PMC NF	VC	PMC	PMC NF	VC
OLR	4.1 ± 1.6	5.7 ± 2.5	5.4 ± 1.4	4.5 ± 2.3	5.3 ± 2.0	3.5 ± 2.2
Freq. domain LNLCSF	3.5 ± 1.3	4.3 ± 1.7	4.0 ± 1.3	1.4 ± 1.0	1.7 ± 0.9	1.9 ± 1.3
Time domain LNLCSF	3.4 ± 1.2	4.2 ± 1.3	4.0 ± 1.3	1.6 ± 1.2	1.7 ± 0.8	1.9 ± 1.3

[a] The group of participants was different at 3 T and at 7 T. PMC – primary motor cortex; PMC NF – primary motor cortex with feedback; VC – visual cortex.

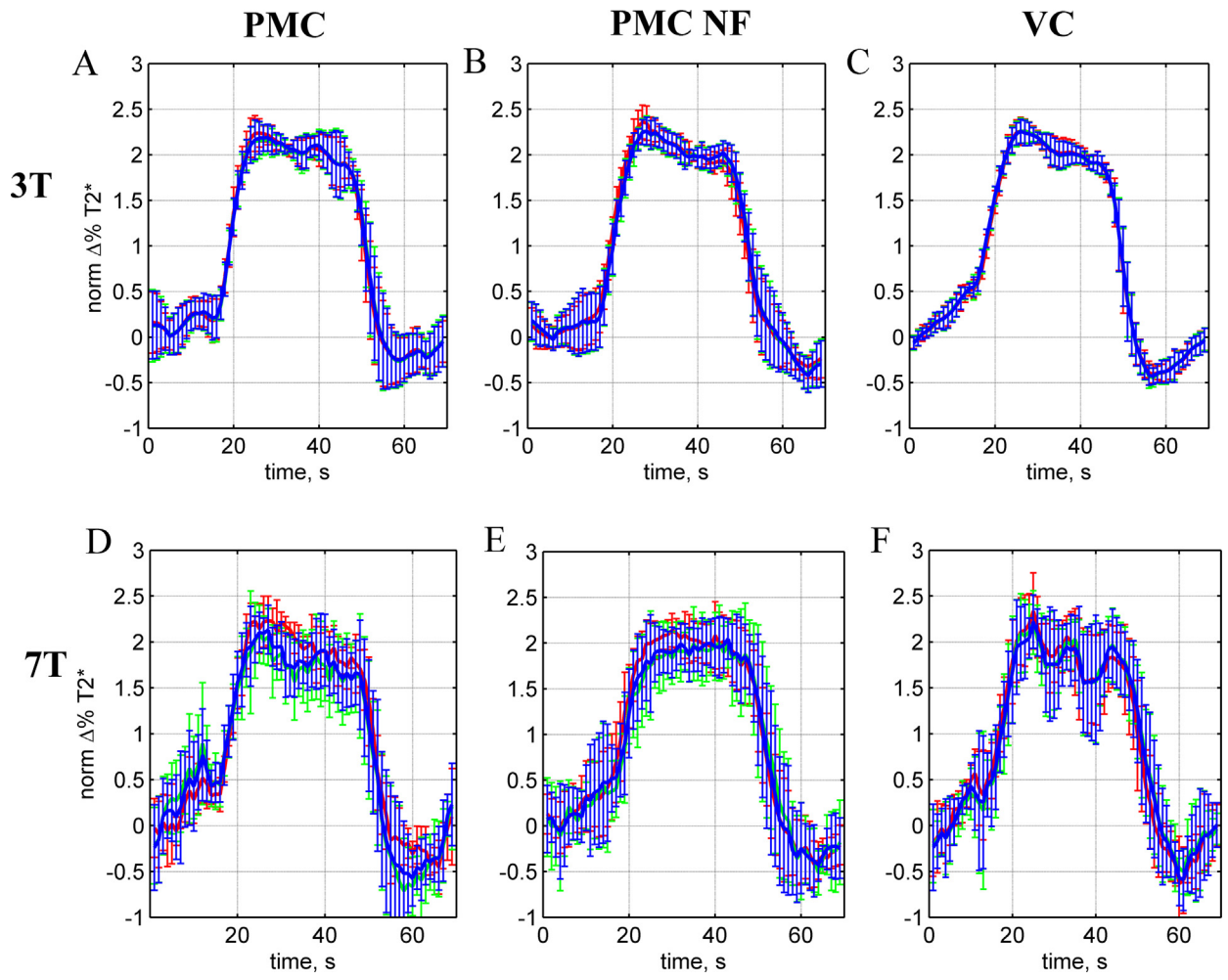

Fig. 5. Event-related group averages of relative T2* change. A high consistency for averaged responses of the activation blocks were observed for PMC (A, D), PMC NF (B, E), and VC (C, F) at 3 T (A, B, C) and 7 T (D, E, F). No bias emerged for the different fitting procedures OLR (red), the automated frequency domain LNLCSF (green), and the automated time domain LNLCSF (blue) T2* estimators; only slight differences in the SD. The event-related averages are highly similar between 3 T and 7 T. Only SDs differences are more marked in the 7 T datasets. Vertical bars represent SD across the group at each time point. OLR – optimized linear regression, LNLCSF – lorentzian non-linear complex spectral fit, PMC – primary motor cortex, PMC NF – primary motor cortex with feedback, VC – visual cortex, SD – standard deviation. (For interpretation of the references to color in this figure legend, the reader is referred to the web version of the article.)

4.1. Explicit T2 estimation at 3 T and at 7 T*

Benefits of the ultra-high magnetic field for spectroscopy acquisitions were addressed elsewhere (e.g. Ugurbil et al., 2003; Tkac et al., 2009), and the direct comparison between acquired 3 T and 7 T data was beyond the scopes of the present research. One of our goals was to assess the potential benefits of the individual and precise T2* estimation (OLR approach) for real-time fSVPS at high and ultra-high magnetic fields. We found that measured T2* average values at 3 T (41.5–54.5 ms) and at 7 T (16.1–17.5 ms) were similar to previous findings, i.e. approximately 40–60 ms at 3 T and 5–40 ms at 7 T (Table 1; Duong et al., 2003; Peters et al., 2007; van der Zwaag et al., 2009). The choice of the voxel size strongly affects fSVPS sensitivity and spatial specificity. For the present study, we selected a relatively small voxel (0.7–1.7 cm^3), which provided sufficient spectral quality for water proton fSVPS. In our study the between-subject variance of T2* was greater at 7 T than at 3 T. This was most probably due to the higher sensitivity to artifacts and lower stability of the 7 T MR system. The changes of line width induced by the BOLD effect were approximately 0.33 ± 0.15 Hz at 3 T and 0.97 ± 0.73 Hz at 7 T. This is somewhat higher than in previous results, which found a line width of about 0.2–0.3 Hz at 4 T (Zhu and Chen, 2001). When comparing 3 T and 7 T, the line width increased approximately by the factor 3.9 in the PMC and by the factor 1.6 in the VC. Compared to previous studies, this is somewhat higher in the PMC, but it is in good agreement with a factor 1.5 increase in the VC when comparing 4 T to 7 T (Tkac et al., 2009). Considering the larger absolute linewidth at 7 T, no gain in the relative change of line width, in T2*, or in the FID signal was observed in our ultra-high field measurements.

The *t*-statistics, CNRs and percent signal changes indicate that real-time fSVPS is feasible at 3 and at 7 T (Fig. 4, Tables 2–4). Both absolute values of the quality measures and their standard deviations lie within a range that is suitable for real-time applications. Again, performance on the 3 T scanner was somewhat better than on the 7 T scanner, i.e. higher *t*-values, higher CNRs, and higher percent signal changes. Moreover, we found higher between-subject variance of the event-related averages on the 7 T scanner (Figs. 4 and 5). Also between ROIs and experimental conditions was the variance larger at 7 T. In a similar vein, the linear regression lengths of the PMC and the PMC NF condition showed high temporal variations only at 7 T (Koush et al., 2011). The variation of regressions lengths in the PMC and the PMC NF conditions

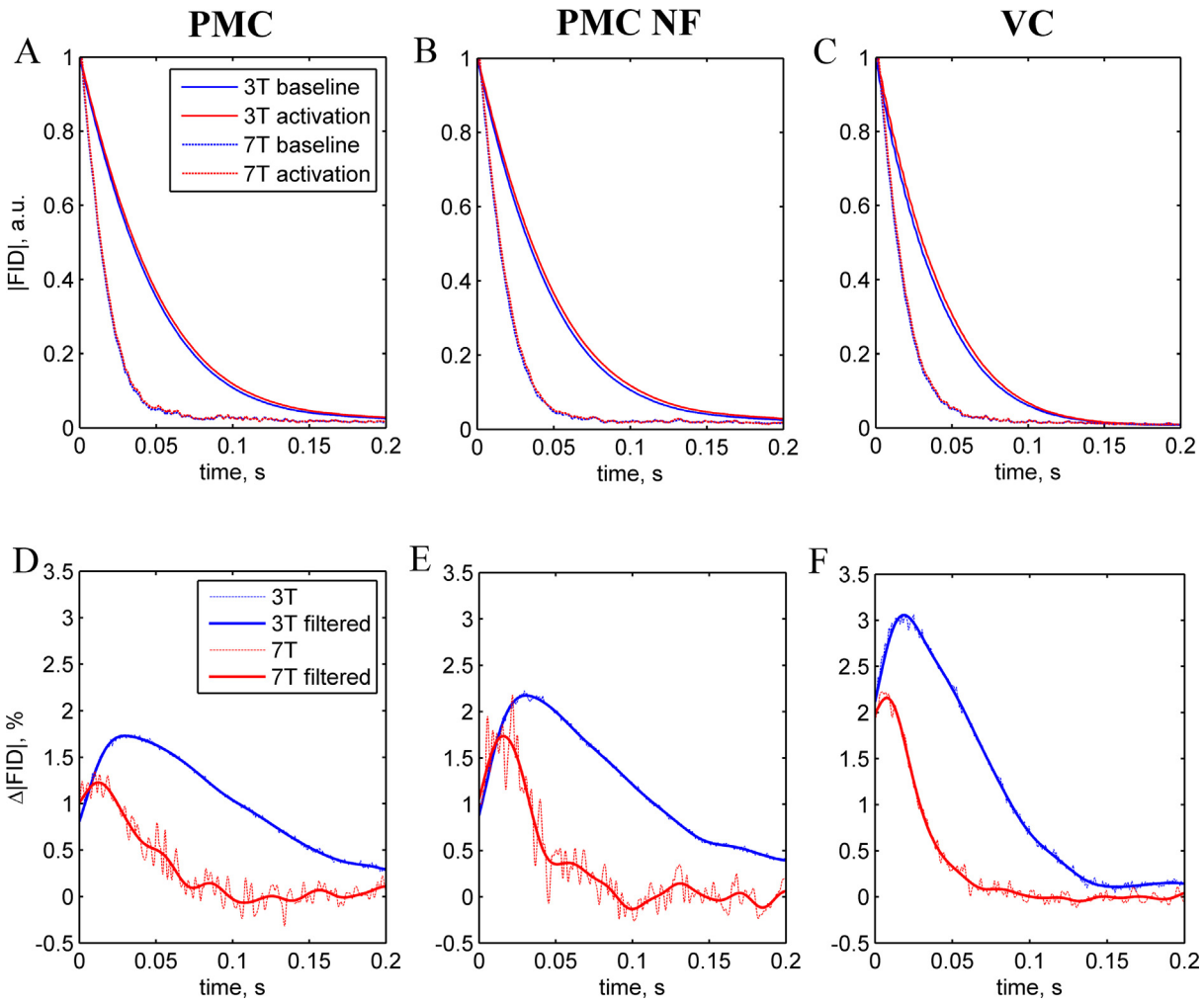

Fig. 6. Preprocessed FIDs at 3 and 7 T normalized and averaged across the group. FID slopes were estimated per condition, i.e. separately for baselines (blue lines) and activation blocks (red lines). Time courses of the PMC (A, D), the PMC NF (B, E) and the VC (C, F) condition were averaged across participants at 3 T (upper solid lines) and 7 T (lower dotted lines). To illustrate the BOLD effect sensitivity, the difference between the corresponding activation (red) and baseline (blue) curves is shown (D–F). The sensitivity curves (D–F; dashed curves) were zero-phase filtered (bold curves; Butterworth low-pass filter, $Fc_{3T} = 0.03$ Hz, $Fc_{7T} = 0.02$ Hz; order = 5). Note that the data from the 7 T scanner showed a faster FID decay rate. Additionally, FID offsets and decay rates display the ROI specific differences between PMC and VC time courses (see also Table 1). BOLD – blood oxygen level dependent, FID – free induction decay, OLR – optimized linear regression, LNLCSF – lorentzian non-linear complex spectral fit, PMC – primary motor cortex, PMC NF – primary motor cortex with feedback, VC – visual cortex. (For interpretation of the references to color in this figure legend, the reader is referred to the web version of the article.)

differed from the VC condition, which exhibited much smaller temporal variations (Fig. 6). The ROI specific differences at 7 T were also apparent when comparing |*FID*| decay rates and |*FID*| amplitudes at time TE (Fig. 6D–F).

The differences between the results from the 3 T and the 7 T scanner might be due to differences in the experimental setup (e.g. different HF coils), larger local field inhomogeneity (hence larger width of the water peak and nonlinear spectral noisiness; see Fig. 2), temporal instabilities (Fig. 6), or they may arise because the 7 T acquisitions were sensitive to a different component of the BOLD signal. Previous studies suggested that intra and extravascular components contribute differently to the BOLD signal changes depending on the acquisition technique, the magnetic field strength, and the echo time (Zhu and Chen, 2001; Duong et al., 2003; Ugurbil et al., 2003). This raises the possibility that using a spin-echo fSVPS acquisition even at relatively short echo-times, extra- and intravascular components from large vessels that normally contribute to the BOLD signal at 3 T are suppressed at 7 T. Such effects have been observed for SE fMRI (Duong et al., 2003; Ugurbil et al., 2003; Hulvershorn et al., 2005; Budde et al., 2013). Thus, the FID amplitude was also modulated by the amplitude at the beginning of the sampling (I_0). In our data this was influenced by T2 (and T1), however, the estimated T2 change (about 0.2%) was much smaller than the change in T2* even at 7 T. Such a mixed T2*/T2 effect might also contribute to the estimated parameter differences as well as the quality measure differences between 3 T and 7 T.

Nevertheless, the absolute change of the line width was 3-fold higher at 7 T, thus demonstrating the potentially higher sensitivity. This could be fully exploited when local field homogeneities are corrected, or by using smaller voxel sizes.

4.2. Comparison of the T2* estimations

In the present study, we compared three different approaches that allow for a direct real-time T2* estimation: the OLR approach, the automated frequency domain LNLCSF approach, and the automated time domain LNLCSF approach. The OLR approach permits an evaluation of the T2* changes in real-time, and provides a reliable feedback signal at 3 and at 7 T (Koush et al., 2011). However,

it requires an additional fSVPS localizer to obtain an optimal linear regression length (Koush et al., 2011).

The automated time domain water peak LNLCSF approach allows an individual, direct, and localized T2* approximation which is suitable for real-time fSVPS neurofeedback. It does not require a spectroscopy localizer and statistical optimizations which are necessary for OLR. Further, LNLCSF requires minimal parameter adjustment, and only needs to be configured once for a particular magnetic field strength and for a particular acquisition protocol. This allows the experimenter to begin directly with the neurofeedback run and therefore considerably reduces the duration of the experiment. Our results showed that the OLR and the LNLCSF approach are both suitable for fitting spectral data in real-time, and that they both provide high quality feedback signals. For most of the time courses at 3 T, the quantified *t*-values and the CNRs were comparable between the OLR and the LNLCSF approaches (Fig. 4; Tables 3–5). However, at 7 T the percent signal changes that were estimated using the OLR approach were much higher than those of the LNLCSF approach. This suggests that the LNLCSF approach provides a mathematically feasible, but not always physiologically optimal parameterization which nevertheless results in high CNRs and *t*-values (Fig. 4). We addressed this effect by applying multiple lorentzian line parameterizations, but the results did not improve (see also Singh et al., 1996; Mierisova and Ala-Korpela, 2001). Our spectroscopy data preprocessing steps allowed for a high convergence rate of the nonlinear fitting algorithm of less than 10 ms at 3 and at 7 T. Due to the relatively small spectroscopy data sample that was evaluated for each update of the feedback signal (TR = 1 s), the processing time to derive the T2*-sensitive feedback signal after the spectrum was acquired was less than 50 ms.

Overall, the automated time domain LNLCSF showed a performance comparable to that of the OLR at 3 T, and one that is somewhat worse than the OLR at 7 T. Given the advantages of the LNLCSF approach (no extra localizer spectroscopy run and minimum parameter adjustment), it nevertheless is a suitable method for real-time fSVPS and can be further optimized for neurofeedback applications. The frequency domain LNLCSF can estimate T2* directly, but the estimation precision suffers from the complex value conversions (real and imaginary parts of the complex spectra were parameterized separately). However, the time domain LNLCSF can assess T2* more explicitly, showed better statistics, and requires only little additional computation time. Automated LNLCSF parameterization provides multiple estimation parameters such as the spectral height, width, and area of a given spectral peak. For the present study, we only reported results from the water peak spectral width estimate because it provides a direct and more precise estimate of T2*. However, spectral height led to a comparable but slightly less sensitive estimation of the BOLD induced dynamics at 3 T. At 7 T, the estimation sensitivity of spectral height was further reduced (results not shown). Additionally, we found that the spectral parameterization resulted in higher CNRs and *t*-statistics of the estimated T2* time courses (results not shown) compared to those extracted from the raw spectral height or width (Zhu and Chen, 2001).

4.3. Recent advances of fSVPS and MRS that can be beneficial for real-time functional MRS

Real-time fSVPS may allow for tissue-specific and metabolite specific neurofeedback. However, due to the large ($\sim 10^3$–10^5) concentration differences between water and metabolites, the use of estimated metabolite peak parameters as a neurofeedback signal will require further optimization of the real-time processing. Moreover, water peak parameterization can be potentially used to enhance the metabolites quantification precision accounting for an exact BOLD spectra shift (Mangia et al., 2006).

Recent advances in MRS now make it possible to map metabolites with small voxel sizes of $\sim 1.5\ cm^3$ with J-resolved techniques (Posse et al., 2009; Jensen et al., 2009; Posse et al., 2007; Tsai et al., 2007), which can be potentially used for metabolite based functional neurofeedback. Furthermore, the J-resolved technique allows a more accurate estimation of the targeted metabolites than the classical PRESS (Bottomley, 1987) and MEGA-PRESS (Mescher et al., 1998) techniques. However, limited SNR of these techniques restricts their application to real-time spectroscopy and neurofeedback.

Other recent developments that could be used to increase the MRS spectral quality in real-time studies deal with head-motion artifacts. Recently developed navigator techniques with dynamic frequency and shim corrections allow for the compensation of head motions, thereby mitigating associated spectral distortions (Keating and Ernst, 2012; Keating et al., 2010; Hess et al., 2011; Zaitsev et al., 2010). In principle, this can also be adapted for use in real-time.

4.4. Limitations

The current research explores only a limited set of parameters. TE and TR were chosen in a pragmatic fashion. Improvements of sensitivity due to a higher acquisition rate with fSVPS and at 7 T were not taken into account. Therefore, the direct comparisons between 3 and 7 T data should be considered with care. Given that the movement related signal changes we observed with our methods were similar to those usually obtained with conventional fMRI (Weiskopf et al., 2004; Weiskopf, 2012), we suggest that our method is as sensitive and thus as suitable for neurofeedback based on mental tasks. Future research may address this comparison more precisely. Because inclusion of early echo components has been shown to be of benefit for reducing noise sources of the BOLD contrast (e.g. Bright and Murphy, 2013; Buur et al., 2009), fSVPS with a relatively short TE may achieve higher SNR, may be more selective to BOLD changes, and may suppress other signal fluctuations at a short TE. Moreover, multi-echo EPI would have allowed for mapping of T2* values and a direct comparison with the single-voxel spectroscopic data. Multi-echo EPI may also reduce EPI associated artifacts (Weiskopf et al., 2005; Mathiak et al., 2002, 2004). Future research may address this comparison among others to elucidate partial volume effects.

5. Conclusions

We automatized the fSVPS-based approach for real-time functional BOLD studies at 3 and at 7 T magnetic fields. We investigated different single water peak parameterization approaches for providing an automated, precise, reliable, and robust feedback signal. However, in order to fully take advantage of ultra-high magnetic fields, improved field homogeneity, stability, and reduced voxel sizes are required. The stability and robustness of the proposed parameterization was demonstrated with the BOLD T2* estimates, and time courses quality measures at 3 and 7 T. The automated LNLCSF approach was suitable for real-time applications.

Acknowledgements

The authors thank H. Hariharan, CMROI, University of Pennsylvania for helpful discussions. This study was supported by the DFG (MA2631/4-1 and IRTG1328), the NIH (RR02305), the Swiss

National Science Foundation, the European Union, and the Center for Biomedical Imaging (CIBM).

References

Alger JR. Quantitative proton magnetic resonance spectroscopy and spectroscopic imaging of the brain: a didactic review. Top Magn Reson Imaging 2010;21(2):115–28.

Bartha R, Drost DJ, Menon RS, Williamson PC. Comparison of the quantification precision of Human short echo time ^{1}H spectroscopy at 1.5 and 4.0 Tesla. Magn Reson Med 2000;44:185–92.

Bottomley PA. Spatial localization in NMR spectroscopy in vivo. Ann N Y Acad Sci 1987;508:333–48.

Bray S, Shimojo JP, O'Doherty JP. Direct instrumental conditioning of neural activity using functional magnetic resonance imaging-derived reward feedback. J Neurosci 2007;27:7498–507.

Bright MG, Murphy K. Removing motion and physiological artifacts from intrinsic BOLD fluctuations using short echo data. Neuroimage 2013;64:526–37.

Budde J, Shajan G, Zaitsev M, Scheffler K, Pohmann R. Functional MRI in Human Subjects with Gradient-Echo and Spin-Echo EPI at 9.4 T. Magn Reson Med 2013 [epub ahead of print].

Buur PF, Poser BA, Norris DG. A dual echo approach to removing motion artefacts in fMRI time series. NMR Biomed 2009;22:551–60.

Caria A, Veit R, Sitaram R, Lotze M, Weiskopf N, Grodd W, et al. Regulation of anterior insular cortex activity using real-time fMRI. Neuroimage 2007;35:1238–46.

Cui X, Bray S, Reiss AL. Functional near infrared spectroscopy (NIRS) signal improvement based on negative correlation between oxygenated and deoxygenated hemoglobin dynamics. Neuroimage 2009;49:3039–46.

deCharms RC, Maeda F, Glover GH, Ludlow D, Pauly JM, Soneji D, et al. Control over brain activation and pain learned by using real-time functional MRI. Proc Natl Acad Sci USA 2005;102:18626–31.

deCharms RC. Applications of real-time fMRI. Nat Rev Neurosci 2008;9(9):720–9.

Deelchand DK, Van De Moortele PV, Adriany G, Iltis I, Andersen P, Strupp JP, et al. In vivo ^{1}H NMR spectroscopy of the human brain at 9.4 T: initial results. J Magn Reson 2010;206:74–80.

Duong TQ, Yacoub E, Adriany G, Hu X, Ugurbil K, Kim SG. Microvascular BOLD contribution at 4 and 7 T in the human brain: gradient-echo and spin-echo fMRI with suppression of blood effects. Magn Reson Med 2003;49:1019–27.

Ferrari M, Mottola L, Quaresima V. Principles, techniques, and limitations of near infrared spectroscopy. Can J Appl Physiol 2004;29:463–87.

Gati JS, Menon RS, Ugurbil K, Rutt BK. Experimental determination of the BOLD field strength dependence in vessels and tissue. Magn Reson Med 1997;38:296–302.

Haase A, Frahm J, Haenicke W, Matthei D. ^{1}H NMR chemical shift selective (CHESS) imaging. Phys Med Biol 1985;30:341–4.

Haller S, Birbaumer N, Veit R. Real-time fMRI feedback training may improve chronic tinnitus. Eur Radiol 2010;20:696–703.

Hennig J, Ernst T, Speck O. Detection of brain activation using oxygenation sensitive functional spectroscopy. Magn Reson Med 1994;31:85–90.

Hess AT, Tisdal MD, Andronesi OC, Meintjes EM, van der Kouwe AJW. Real-time motion and B0 corrected single voxel spectroscopy using volumetric navigators. Magn Reson Med 2011;66:314–23.

Hulvershorn J, Bloy L, Gualtieri EE, Leigh JS, Elliott MA. Spatial sensitivity and temporal response of spin echo and gradient echo bold contrast at 3 T using peak hemodynamic activation time. Neuroimage 2005;24:216–23.

Jensen JE, Licata SC, Ongur D, Friedman SD, Prescot AP, Henry ME, et al. Quantification of J-resolved proton spectra in two-dimensions with LCModel using GAMMA-simulated basis sets at 4 Tesla. NMR Biomed 2009;22:762–9.

Johnston SJ, Boehm SG, Healy D, Goebel R, Linden DEJ. Neurofeedback: a promising tool for the self-regulation of emotion networks. Neuroimage 2010;49:1066–72.

Keating B, Ernst T. Real-time dynamic frequency and shim correction for single-voxel magnetic resonance spectroscopy. Magn Reson Med 2012;68(5):1339–45.

Keating B, Deng D, Roddey JC, White N, Dale A, Stenger VA, et al. Prospective motion correction for single-voxel ^{1}H MR spectroscopy. Magn Reson Med 2010;64:672–769.

Klose U. In vivo proton spectroscopy in presence of eddy currents. Magn Reson Med 1990;14:26–30.

Koush Y, Zvyagintsev M, Dyck M, Mathiak KA, Mathiak K. Signal quality and Bayesian signal processing in neurofeedback based on real-time fMRI. Neuroimage 2012;59:478–89.

Koush Y, Elliott MA, Mathiak K. Single voxel proton spectroscopy for neurofeedback at 7 Tesla. Materials 2011;4:1548–63.

Marshall I, Higinbotham J, Bruce S, Freise A. Use of voigt lineshape for quantification of in vivo ^{1}H spectra. Magn Reson Med 1997;37:651–7.

Mangia S, Tkac I, Gruetter R, Van De Moortele PF, Giove F, Maraviglia B, et al. Sensitivity of single-voxel ^{1}H-MRS in investigating the metabolism of the activated human visual cortex at 7 T. Magn Reson Imaging 2006;24:343–8.

Mathiak K, Rapp A, Kircher TTJ, Grodd W, Hertrich I, Weiskopf N, et al. Mismatch responses to randomized gradient switching noise as reflected by fMRI and whole-head magnetoencephalography. Hum Brain Mapp 2002;16:190–5.

Mathiak K, Hertrich I, Grodd W, Ackermann H. Discrimination of temporal information at the cerebellum: functional magnetic resonance imaging of non-verbal auditory memory. NeuroImage 2004;21:154–62.

Mathiak KA, Koush Y, Dyck M, Gaber TJ, Alawi E, Zepf FD, et al. Social reinforcement can regulate localized brain activity. Eur Arch Psychiatry Clin Neurosci 2010;260(2):132–6.

Mierisova S, Ala-Korpela M. MR spectroscopy quantitation: a review of frequency domain methods. NMR Biomed 2001;14:247–59.

Mescher M, Merkle H, Kirsch J, Garwood M, Gruetter R. Simultaneous in vivo spectral editing and water suppression. NMR Biomed 1998;11:266–72.

Mulkern RV, Chen N, Oshio K, Panych LP, Rybicki FJ, Gambarota G. Fast spectroscopic imaging strategies for potential imaging applications in fMRI. Magn Reson Imaging 2004;22:1395–405.

Nacewiz MB, Angelos L, Dalton KM, Fischer R, Anderle MJ, Alexander AL, et al. Reliable non-invasive measurement of human neurochemistry using proton spectroscopy with an anatomically defined amygdala-specific voxel. Neuroimage 2012;59(3):2548–59.

Oldfield RC. The assessment and analysis of handedness: the Edinburgh inventory. Neuropsychologia 1971;9:97–113.

Peters AM, Brookes MJ, Hoogenraad FG, Gowland PA, Francis ST, Morris PG, et al. T2* measurements in human brain at 1.5, 3 and 7 T. Magn Reson Imaging 2007;25:748–53.

Posse S, Fitzgerald D, Gao K, Habel U, Rosenberg D, Moore GJ, et al. Real-time fMRI of temporolimbic regions detects amygdala activation during single-trial self-induced sadness. Neuroimage 2003;18(3):760–8.

Posse S, Otazo R, Caprihan A, Bustillo J, Chen H, Henry PG, et al. Proton echo-planar spectroscopic imaging of J-coupled resonances in human brain at 3 and 4 Tesla. Magn Reson Med 2007;58(2):236–44.

Posse S, Otazo R, Tsai SY, Yoshimoto AE, Lin FH. Single-shot magnetic resonance spectroscopic imaging with partial parallel imaging. Magn Reson Med 2009;61:541–7.

Provencher SW. Automatic quantitation of localized in vivo ^{1}H spectra with LCModel. NMR Biomed 2001;14:260–4.

Richards TL, Dager SR, Posse S. Functional MR spectroscopy of the brain. Neuroimaging Clin N Am 1998;8:823–4.

Rota G, Sitaram R, Veit R, Erb M, Weiskopf N, Dogil G, et al. Self-regulation of regional cortical activity using real-time fMRI: the right inferior frontal gyrus and linguistic processing. Hum Brain Mapp 2009;30:1605–14.

Ruiz S, Lee S, Soekadar SR, Caria A, Veit R, Kircher T, et al. Acquired self-control of insula cortex modulates emotion recognition and brain network connectivity in schizophrenia. Hum Brain Mapp 2013;34(1):200–12.

Schafer A, Van der Zwaag W, Francis ST, Head KE, Gowland PA, Bowtel RW. High resolution SE-fMRI in humans at 3 and 7 T using a motor task. Magn Reson Mater Phy 2008;21:113–20.

Scharnowski F, Josephs HC, Weiskopf O, Rees NG. Improving visual perception through neurofeedback. J Neurosci 2012;32:17830–41.

Shibata K, Watanabe T, Sasaki Y, Kawato M. Perceptual learning incepted by decoded fMRI neurofeedback without stimulus presentation. Science 2011;9(334):1413–5.

Singh M, Patel P, Khosla D. Estimation of T2* in functional spectroscopy during visual stimulation. IEEE Trans Nucl Sci 1996;43:2037–43.

Subramanian L, Hindle JV, Johnston S, Roberts MV, Husain M, Goebel R, et al. Real-time functional magnetic resonance imaging neurofeedback for treatment of Parkinson's disease. J Neurosci 2011;31(45):16309–17.

Tkac I, Gruetter R. Methodology of ^{1}H NMR spectroscopy of the human brain at very high magnetic fields. Appl Magm Reson 2005;29:139–57.

Tkac I, Öz G, Adriany G, Ugurbil K, Gruetter R. In vivo ^{1}H NMR spectroscopy of the human brain at high magnetic fields: metabolite quantification at 4 T vs 7 T. Magn Reson Med 2009;62:868–79.

Tsai SY, Posse S, Lin YR, Ko CW, Otazo R, Chung HW, et al. Fast mapping of the T2 relaxation time of cerebral metabolites using proton echo-planar spectroscopic imaging (PEPSI). Magn Reson Med 2007;57:859–65.

Ugurbil K, Adriany G, Andersen P, Chen W, Garwood M, Gruetter R, et al. Ultra-high field magnetic resonance imaging and spectroscopy. Magn Reson Imaging 2003;21:1263–81.

van den Boogaart A, Ala-Korpela M, Jokisaari J, Griffiths JR. Time and frequency domain analysis of NMR data compared: an application to 1D ^{1}H spectra of lipoproteins. Magn Reson Med 1994;31:347–58.

van der Veen JWC, Weinberger DR, Tedeschi G, Frank JA, Duyn JH, Proton MR. Spectroscopic imaging without water suppression. Radiology 2000;217:296–300.

van der Zwaag W, Francis S, Head K, Peters A, Gowland P, Morris P, et al. fMRI at 1.5, 3 and 7 T: characterising BOLD signal changes. NeuroImage 2009;47:1425–34.

Weiskopf N, Klose U, Birbaumer N, Mathiak K. Single line imaging spectroscopy (SLIMS): exploring the fMRI signal. Proc Intl Soc Mag Reson Med 2003:11.

Weiskopf N, Scharnowski F, Veit R, Goebel R, Birbaumer N, Mathiak K. Self-regulation of local brain activity using real-time functional magnetic resonance imaging (fMRI). J Physiol 2004;98:357–73.

Weiskopf N, Klose U, Birbaumer N, Mathiak K. Single-shot compensation of image distortions and BOLD contrast optimization using multi-echo EPI for real-time fMRI. NeuroImage 2005;24:1068–79.

Weiskopf N, Sitaram R, Josephs O, Veit R, Scharnowski F, Goebel R, et al. Real-time functional magnetic resonance imaging: methods and applications. Magn Reson Imaging 2007;25:989–1003.

Weiskopf N. Real-time fMRI and its application to neurofeedback. Neuroimage 2012;62(2):682–92.

Yacoub E, Duong TQ, Van de Moortele PF, Lindquist M, Adriani G, Kim SG, et al. Spin-echo fMRI in humans using high spatial resolutions and high magnetic fields. Magn Reson Med 2003;49(4):655–64.

Yoo SS, O'Leary HM, Fairneny T, Chen NK, Panych L, Park H, et al. Increasing cortical activity in auditory areas through neurofeedback functional magnetic resonance imaging. Neuroreport 2006;17(12):1273–8.

Zaitsev M, Speck O, Hennig J, Büchert M. Single-voxel MRS with prospective motion correction and retrospective frequency correction. NMR Biomed 2010;23:325–32.

Zhu X, Chen W. Observed BOLD effects on cerebral metabolite resonances in human visual cortex during visual stimulation: a functional ^{1}H MRS study at 4 T. Magn Reson Med 2001;46:841–7.

Zotev V, Krueger F, Phillips R, Alvarez RP, Simmons WK, Bellgowan P, et al. Self-regulation of amygdala activation using real-time FMRI neurofeedback. PLoS ONE 2011;6(9):e24522.